

Complex Analysis of Rupture Risk of Intracranial Saccular Aneurysms upon Hemodynamic and Geometric Parameters

KRZYSZTOF SZAFRAŃSKI*

Szczecin University of Technology, Faculty of Electrical Engineering, Szczecin, Poland

The paper includes a new concept of assessment of rupture risk of intracranial saccular aneurysms using geometric and hemodynamic parameters of aneurysm, artery and blood. Previous decision systems are mainly based on the size of aneurysm and frequency of subarachnoid hemorrhages, therefore after performing simulation tests it has been proved that the complex assessment of clinical cases is possible thanks to evaluation of shape and size coefficient of a secondary aneurysm occurring on the surface of a primary aneurysm, width of a primary aneurysm neck, curvature of an artery on which a primary aneurysm is located and the size of blood impingement area at artery wall. The paper contains results of the simulation tests of blood flow in the primary and secondary aneurysm, as well as verification of proposed criteria of rupture risk assessment for 5 clinical cases.

K e y w o r d s: aneurysm, artery curvature, Womersley velocity profile, rupture risk assessment, tensile stress, decision-making system

1. Introduction

Intracranial saccular aneurysm is a pathological bulge of the cerebral artery. It is mostly located on the weakened artery wall where it gradually grows until a sac of 5 to 10 mm is formed, although the size may exceed 25 mm. Aneurysms are supposed to occur at 2 to 5% population, whereas 15 to 20% patients have multiple intracranial aneurysms. Aneurysms are usually detected as a result of rupture leading to the subarachnoid hemorrhage or even to the cerebral ventricle hemorrhage. In case of the subarachnoid hemorrhage, the risk of death is from 30 to 50% [1]. Moreover, it is estimated that 9–16 per 100 000 people can suffer aneurysm rupture within life-span.

* Correspondence to: Krzysztof Szafranski, Szczecin University of Technology, Faculty of Electrical Engineering, ul. 26 Kwietnia 10, 71-126 Szczecin, e-mail: kris790@wp.pl

Received 05 May 2008; Accepted 19 September 2008

The clinical evidence shows that mainly larger aneurysms are prone to rupture, however, it happens that aneurysms of diameter less than 5 mm rupture whereas aneurysms of diameter more than 10 mm are intact for a long time [2, 3, 4]. Thereby, evaluation of the rupture risk of aneurysms solely on the basis of size criterion shall not be helpful in planning of the treatment by neurosurgeons [5].

Autopsies often proved presence of unruptured aneurysms at patients whose cause of death was different [6, 7]. A surgical intervention, e.g. clipping of the aneurysm neck, involves a risk of post-operative complications [8, 9], and intra-vascular embolisation is not always efficient due to numerous cases of movement of coils from the aneurysm into aorta. Therefore, the rupture risk of the intracranial aneurysms is also assessed using of the parametric relations based upon the geometry of aneurysm and artery, as well as dynamic properties of blood flow. The main objective of all hemodynamic researches is specifying of criteria for evaluation of the rupture risk of aneurysms in order to minimise the number of surgical interventions. The researches are performed by means of CFD software for analysis of dynamics of blood flow (the most often used software is Fluent packet) [10–15] and hydraulic and mechanic systems that simulate aneurysm, and artery and blood environment [16–19]. Some parameters, such as blood velocity, are calculated using the systems involving the Doppler effect [20, 21]. The source of data necessary for creating models of aneurysms by means of CFD software are CT [22, 23, 24] and MRI images [25, 26].

Making a decision for treatment of the intracranial aneurysms triggers making a choice between consequences of surgery and long-term rupture risk of aneurysm. The biggest obstacle in the decision-making process is a relatively long period of acquisition of data necessary for making the decision and difficulty in generalisation of the obtained results for every patient due to a considerable quantity of analysed parameters. The decision analysis firstly requires defining of the factors contributing to rupture of aneurysm, then evaluating the parameters describing the factors and probability of occurrence of the specific parameter values, and finally comparison of every factor in aspect of its impact on the decision-making process. In previous years various medical decision analyses were performed, including several studies for the unruptured aneurysms [27–31].

The analysis of the above mentioned ideas of the decision systems proves that they are solely based on statistical data for selected age groups including only the fact of rupture of aneurysm, subarachnoid hemorrhage and average values of the rupture risk of different aneurysm classes or occurrence of post-operative complications for every age group, and the most often used parameter in classification of the rupture risk of aneurysms is the size.

Therefore, upon published results of researches, it can be proposed that estimation of the selected parameters of the intracranial aneurysms using the mathematical model involving shape and hemodynamics of blood flow in artery and aneurysm can support neurosurgeons in the decision-making process related to the aneurysms.

It has been observed that assessment of the following parameters is especially essential for neurosurgeons:

- Coefficient of shape and coefficient of size of the secondary aneurysm forming on the surface of primary aneurysm;
- Width of the primary aneurysm neck;
- Degree of curvature of the artery, on which the primary aneurysm is located.

2. Analysis of the Rupture Risk of the Secondary Aneurysm

The clinical researches prove that enlargement of the intracranial aneurysms is the consequence of forming of so called “blebs” or “lobulations” on the surface of primary aneurysms [32, 33]. In 60s Crompton found that the secondary aneurysms formed on the surface of 57% ruptured aneurysms and only 16% unruptured aneurysms [34]. Moreover, the researches made by Sampei [35] showed that 75% unruptured aneurysms with a bleb on the surface ruptured within 1 to 10 months since detection of the primary aneurysm, whereas just 20% aneurysms without bleb on the surface ruptured within the same period of time. The neurosurgeon practice shows that the secondary aneurysm is a potential health hazard and shall be immediately treated, and if surgery is not recommended, the follow-up tests, i.e. CT or MRI, shall be performed regularly.

The stability problem of the intracranial aneurysms was also described by Steiger [36], who noticed that formation of the secondary aneurysm on the weaker aneurysm wall changed stability conditions of the primary aneurysm, and by Meng et al. [37] who explained the process of evolution of the secondary aneurysm by means of Laplace law.

The analysis of the rupture risk of the secondary aneurysm is based on a study of dynamics of wall tensile stress of the primary and the secondary aneurysm [38]. Figure 1 presents the primary aneurysm of $d_p(0)$ wall thickness for $t = 0$ and $d_p(T)$ wall thickness for $t = T$, whereas the secondary aneurysm of $d_w(T)$ thickness formed on the surface of the primary aneurysm. Moreover, the control area B of the primary aneurysm of the same volume as area A where the secondary aneurysm occurred, was shown for $t = 0$. The assumption of the identical rate of growth of the primary and the secondary aneurysm was used for further calculations.

Using the above mentioned assumption, the identical volume of A' and B' area was accepted according to the following formula:

$$2\pi R(T) \cdot \left\{ R(T) - \sqrt{[R(T)]^2 - [l'(T)]^2} \right\} \cdot d_p(T) = 2\pi r(T) \cdot h'(T) \cdot d_w(T) \quad (1)$$

where $R(T)$ is the radius of the primary aneurysm after period T , $r(T)$ is the radius of the secondary aneurysm after period T , $l'(T)$ is half of the orifice of the secondary

aneurysm after period T , $h'(T)$ is the height of the secondary aneurysm after period T , $d_p(T)$ is the thickness of area B' of the primary aneurysm after period T , and $d_w(T)$ is the thickness of area A' of the secondary aneurysm after period T . Equation (1) can be expressed as:

$$\frac{d_w(T)}{d_p(T)} = \frac{R(T)}{r(T)} \cdot \frac{R(T) - \sqrt{[R(T)]^2 - [l'(T)]^2}}{h'(T)}. \quad (2)$$

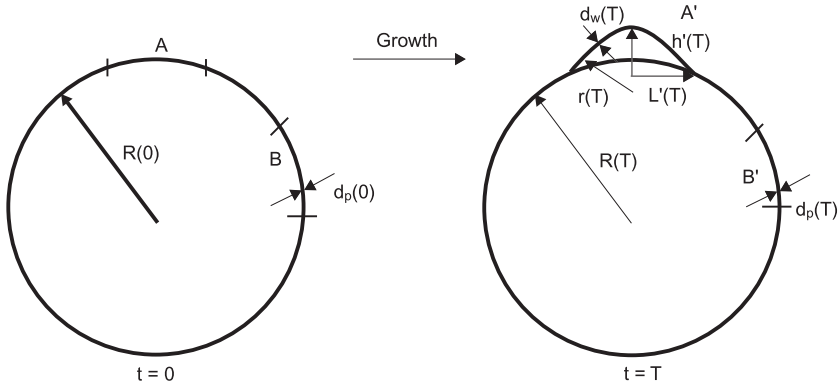


Fig. 1. Forming of the secondary aneurysm at the surface of the primary aneurysm

Considering the fact that wall of the aneurysm is very thin as compared with a radius of the aneurysm, the linear form of Laplace law was applied for the aneurysms according to the following formulas:

$$S_p(T) = \frac{P(T) \cdot R(T)}{2 \cdot d_p(T)} \quad (3)$$

and

$$S_w(T) = \frac{P(T) \cdot r(T)}{2 \cdot d_w(T)} \quad (4)$$

where $S_p(T)$ and $S_w(T)$ are the wall tensile stresses of the primary and the secondary aneurysm after period T , respectively. The relation between the wall tensile stresses can be defined as a relative stress $\eta(T)$ according to the formula (5):

$$\eta(T) = \frac{S_w(T)}{S_p(T)}. \quad (5)$$

Applying the following relation for the secondary aneurysm:

$$[r(T) - h'(T)]^2 + [l'(T)]^2 = [r(T)]^2 \quad (6)$$

the following equation for $\eta(T)$ was derived:

$$\eta(T) = \eta[\mu(T), \lambda(T)] = \frac{\mu(T) \cdot \left\{1 + \sqrt{1 - [\mu(T)]^2}\right\}}{4} \cdot \frac{\left\{1 + [\lambda(T)]^2\right\}^2}{\lambda(T)} \quad (7)$$

where:

$\mu(T) = \frac{l'(T)}{R(T)}$ is the size coefficient of the secondary aneurysm showing

relative width of the neck of the secondary aneurysm as compared with the radius of the primary aneurysm,

$\lambda(T) = \frac{h'(T)}{l'(T)}$ is the shape coefficient of the secondary aneurysm showing

the relation between the height and the neck of the secondary aneurysm.

The wall tensile stress of the aneurysm is one of the main factors increasing the rupture risk of aneurysm, therefore the analysis of the relative stress η as the function of the size coefficient μ and the shape coefficient λ was performed:

$$\eta(\mu, \lambda) = \frac{\mu(1 + \sqrt{1 - \mu^2})}{4} \cdot \frac{(1 + \lambda^2)^2}{\lambda}. \quad (8)$$

The relative stress is the basis for assessment of the rupture risk of aneurysm, and is the function of two non-dimensional parameters, thereby properties of the aneurysm of any size and the rupture risk of aneurysm can be evaluated.

Figure 2 presents the graph of the relative stress as a function of the shape coefficient λ for various values of the size coefficient μ . For a specified value of λ , the relative stress is minimal if $\frac{\partial \eta}{\partial \lambda} = 0$, i.e. for $\lambda = \frac{\sqrt{3}}{3} = 0.577$. The start point of all characteristics is at $\eta=1$, as the secondary aneurysm forms at wall of the primary aneurysm, and during growth of the secondary aneurysm its tensile stress is equal to the tensile stress of the primary aneurysm, therefore the initial value of the relative stress is 1.

The shape of curves in Fig. 2 is typical for evolution of the secondary aneurysm. During growth of the secondary aneurysm two simultaneous processes (phases) occur:

- change of radius r . As the secondary aneurysm grows, its radius decreases until a semi-sphere is formed (parameter λ is equal to 1), and then it increases.
- the wall of the secondary aneurysm is getting thinner. It is caused by limited extensibility of the wall layers of aneurysm.

As for the value of the relative tensile stress, i.e. $\eta \geq 1$, the rupture risk of aneurysm is significantly increased. The walls of the secondary aneurysm are far less

tensile than the walls of the primary aneurysm, thereby the strength of the walls of the secondary aneurysm shall be at most equal to the strength of the walls of the primary aneurysm. It can be anticipated that the rupture occurs when the strengths of the walls of both the primary and secondary aneurysms are identical.

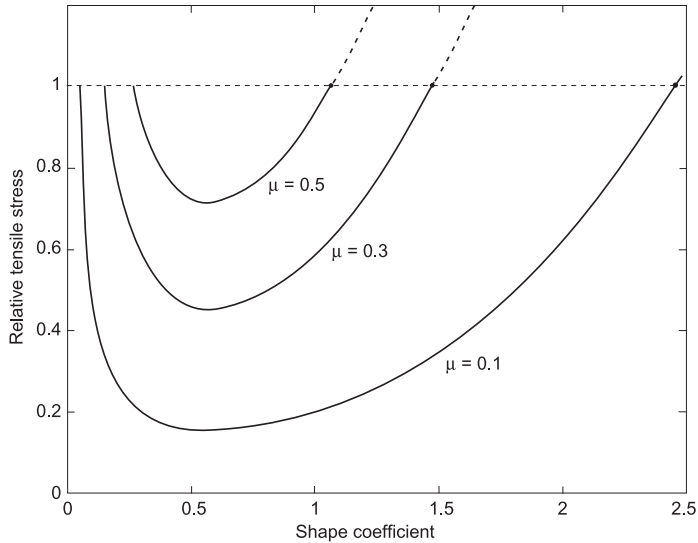


Fig. 2. The graph of the relative tensile stress η as the function of the shape coefficient λ of the secondary aneurysm, concurrent with [37]

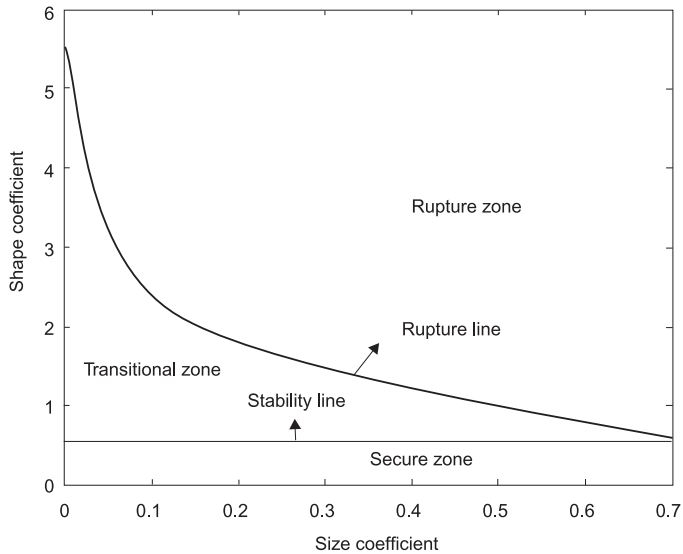


Fig. 3. Rupture risk zones of the secondary aneurysm concurrent with [37]

Three main zones can be separated within aneurysm (as in Fig. 3): the secure, the transitional and the rupture zone. The secure zone is an area of growth of the aneurysm until stability is achieved, i.e. the aneurysm is not prone to the rupture. The transitional zone is a state between the stability of the aneurysm and the rupture, therefore the aneurysms located within the transitional zone must be regularly checked up by means of CT or MRI. The rupture zone is an area located over the rupture line where the aneurysm shall rupture according to the assumptions of the model of the primary and the secondary aneurysm. Upon Figure 3, the prediction of the rupture risk of the intracranial aneurysms can be performed, and treatment for aneurysms within the transitional zone shall be recommended.

3. Simulation Tests of Blood Flow in Artery and Aneurysm

The model of aneurysm on a straight artery is the most often applied model helpful in understanding the process of evolution and growth of aneurysms [39]. However, in clinical practice the aneurysms on straight artery are observed very seldom. Sidewall aneurysms are prevalent and they grow at bifurcations of the arteries and at the artery curvatures. The researches are based on simplified assumptions and cannot reproduce physiological changes within a hemodynamic environment [40, 41]. Therefore, the model of aneurysm on the curved artery has been elaborated, and the detailed analysis of blood flow in the aneurysm and the artery of various curvatures has been performed. Comsol Femlab 3.0, Fluent and STARCD packets were applied in this study for the analysis of blood flow in aneurysms of various neck width located on the arteries of various curvature.

The spherical aneurysm geometry was accepted, and the analysis of hemodynamic properties was performed through variation of the curvature of the aorta and the neck width of the aneurysm for unchanged values of other parameters, i.e. diameter of the aorta and the aneurysm.

Ten models of the sidewall aneurysms were elaborated for the study of influence of the artery curvature on the blood flow profile and the stress distribution [42, 43]. R was accepted as the radius of the aorta curvature, $(1/R)$ as the curvature of aorta, D as the aneurysm diameter, N as the aneurysm neck width, and d as the diameter of aorta. The models were divided into two groups, whereas the first group included six aneurysms R1–R6 of six different artery curvature values, and the other group included four aneurysms N1–N4 of four different neck width values. The diameter of the aorta was accepted as 3 mm, and the aneurysm diameter as 12 mm for all ten models. For the models R1–R6, the artery curvature varied from 0 to 0.1667 mm^{-1} , and the neck width was fixed at 7.5 mm. For the models N1–N4, the neck width varied from 6 to 9.56 mm, and the artery curvature was fixed at 0.0833 mm^{-1} .

Before simulations were performed, the input and output conditions for blood flow were determined. At the input of the artery the complete Womersley profile

was applied (according to the formula 9), and the zero pressure gradient was used at the output of the tested system. The implicit scheme was selected due to its stability even for large numerical steps. The simulations of blood flow at the stable state (for the constant blood flow velocity of $30 \text{ cm}\cdot\text{s}^{-1}$) were interrupted when the defined tolerance (i.e. e^{-5}) was achieved.

$$v_w(t, y) = \frac{2Q_0}{\pi a^2} (1 - y^2) + \sum_{n=1}^{N-1} \frac{Q_n}{\pi a^2} \frac{1 - \frac{J_0(\beta_n y)}{J_0(\beta_n)}}{1 - \frac{2J_1(\beta_n)}{\beta_n J_0(\beta_n)}} e^{i\omega n t} \quad (9)$$

where:

$$\alpha_n \equiv a \sqrt{\frac{\omega n}{\nu}}, \quad \beta_n \equiv \alpha_n i^{\frac{3}{2}}, \quad y \equiv \frac{r}{a}, \quad \omega = \frac{2\pi}{T} \quad (10)$$

$J_0()$ – the Bessel function of the first kind (of the 0 order),

$J_1()$ – the Bessel function of the first kind (of the 1st order),

v_w – velocity of blood flow according to the Womersley profile,

Q_0 – 0-th element of Fourier series representation of blood flow rate,

Q_n – n-th element of Fourier series representation of blood flow rate,

a – radius of blood vessel,

r – apex of blood flow within vessel in Y-axis,

ω – blood pulsation,

n – number of Fourier series coefficients,

ν – kinematic viscosity of blood,

i – imaginary unit,

T – cardiac cycle.

The blood flow rate $Q(t)$ can be approximated by the complex Fourier series, therefore on the basis of data from measurement of the blood flow rate in the carotid artery of a 25-year old patient using Doppler effect [44], the coefficients a_n and b_n of the Fourier series (for the first 4 harmonics) approximating the blood flow rate $Q(t)$ were calculated. FFTPack in Fortran language was applied for the calculations.

It was assumed for the artery and the aneurysm that the period of the simulated blood flow was 1 s correspondent to the heart rate of 60 beats per minute. The maximum flow velocity was so fixed to be equal to the maximum flow velocity of $59.8 \text{ cm}\cdot\text{s}^{-1}$ measured in the carotid artery. Moreover, the kinematic viscosity was accepted as $2.83 \cdot 10^{-6} \text{ m}^2 \cdot \text{s}^{-1}$, and the blood density as $1060 \text{ kg}\cdot\text{m}^{-3}$, whereas the diameter of the carotid artery was 3 mm. These values are physiological for human blood of 37°C temperature and 45% hematocrit.

Figure 4 presents the pulsational blood flow entering the artery and the aneurysm of the Womersley velocity profile. The results obtained during the first and the second heart cycle were not taken into account due to numerical instability within the initial simulation period.

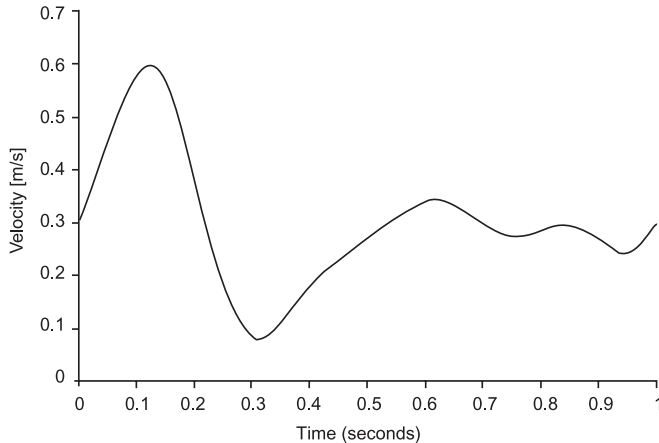


Fig. 4. The pulsational blood flow in an artery and an intracranial aneurysm according to the Womersley velocity profile

The flow simulation in the stable state and the pulsational flow were performed in the Comsol Femlab and the Fluent environment using two Core 2 Duo processors. The observed phenomena are described below [42]:

1) **Flow intensifies as curvature increases.** If the artery curvature is close or equal to 0 (as for the model R1 of the straight artery), then blood enters the aneurysm as a diffusion of viscous particles. The arteries of higher curvature feature the velocity profile directed into the aneurysm sac as the consequence of impact of centrifugal force. Moreover, as the artery curvature increases (as for the model R5 or R6), the area of wall shear stresses moves towards the aneurysm dome (Fig. 5), i.e. the region primarily prone to the rupture, that is in accordance with conclusions in [43, 45]. The numerical values of curvature for six tested aneurysm models are listed in the Table 1 below.

Table 1. Overview of the artery curvature for six aneurysm models of the identical neck width

Aneurysm	Artery curvature $1/R$ (mm^{-1})	Aneurysm neck width N (mm)
R1	0.000	7.500
R2	0.067	7.500
R3	0.083	7.500
R4	0.100	7.500
R5	0.125	7.500
R6	0.167	7.500

2) **The performed tests have proved that the size of blood impingement area varies dynamically during the heart cycle** lasting from about 0.8 to 1 second.

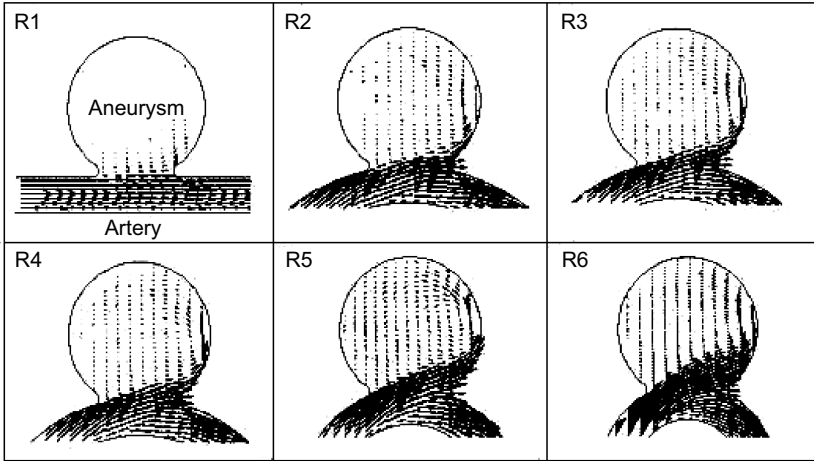


Fig. 5. Comparison of the blood velocity profile for the different aneurysm models of the identical neck width during the maximum systole for the pulsational flow, concurrent with [43]

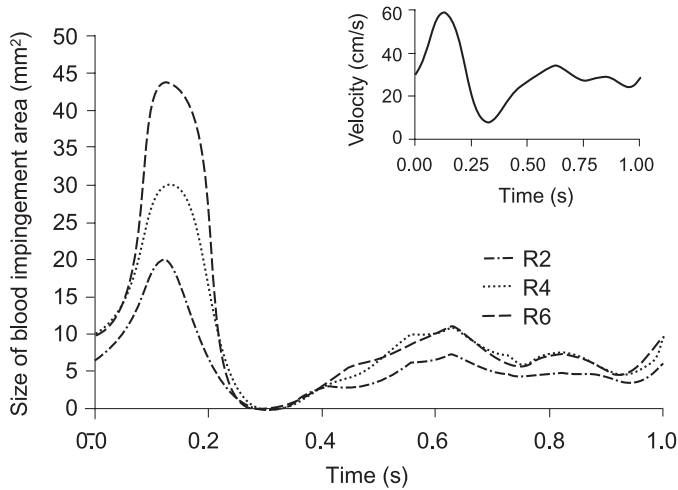


Fig. 6. Dynamic variation of the size of blood impingement area during the heart cycle, concurrent with [43]

The tests were performed for the wall shear stresses exceeding $20 \text{ dyn}\cdot\text{cm}^{-2}$. As for the artery R6 of high curvature (i.e. 0.167 mm^{-1}), variation of the size of blood impingement area was more than twice as for the artery R2 of low curvature (i.e. 0.067 mm^{-1}).

3) **It can be concluded that the size of blood impingement area is the function of artery curvature and aneurysm neck width.** It was noticed that the curvature increase contributed to faster enlargement of the blood impingement area than in

the case of the aneurysm neck width. This observation is proved by the Table 2, e.g. the size of the blood impingement area for aneurysm R4 is larger than for aneurysm N3 considering that the neck width and the artery curvature are similar for both the models. The size of the blood impingement area rises nearly linear with increase of the aorta curvature ($1/R$) and the third order of the aneurysm neck width (N^3).

Table 2. The size of blood impingement area and the value of N^3/R parameter for the models R1-R6 and N1-N4

Aneurysm model	The value of N^3/R (mm ²)	The size of blood impingement area (mm ²)
R1	0	3.4
R2	28.2	20.1
R3	36.7	24.2
R4	42.2	30.5
R5	52.7	40.6
R6	70.5	44.8
N1	17.9	7.8
N2	18.7	12.1
N3	42.5	24.9
N4	72.5	43.6

4) Figure 7 presents the distribution of the blood flow velocity and the wall shear stress for the stable state (the Poiseuille flow) for a Reynolds number corresponding to the maximum systole and for the pulsational flow at the maximum systole.

The distribution of the blood flow velocity and the wall shear stress is similar according to observations of Steiger [46], who noticed that the pulsational flow differed just slightly from the Poiseuille flow during systole, whereas during diastole the pulsational flow was significantly disturbed as compared with the Poiseuille flow.

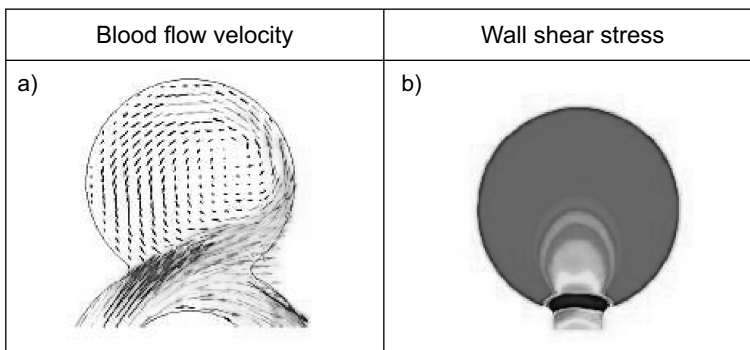


Fig. 7. Distribution of the blood flow velocity (Fig. 7a) and the wall shear stress of the model R6 (Fig. 7b) for the stable state (the Poiseuille flow) and for the pulsational flow at the maximum systole

4. Application of Geometrical and Mechanical Parameters for the Decision-making Process

On the basis of clinical data, the rupture risk for five cases of the primary aneurysm with the secondary aneurysm has been assessed. Selection of such cases is reasonable due to high frequency of rupture of aneurysms with blebs on their surface equal to 0,75. The analysis of the rupture risk of two cases of the primary and the secondary aneurysm is presented below:

4.1. Sidewall Aneurysm of Small Neck Width Located on Artery of High Curvature

Using images from the spiral CT, the following geometrical parameters of the aneurysm and the artery in the initial growth phase of the secondary aneurysm were determined:

- Curvature of the artery on which the primary aneurysm was located: 0.16 mm^{-1} ;
- Width of the primary aneurysm neck: 7.72 mm;
- Radius of the primary aneurysm: 4.8 mm;
- Width of the secondary aneurysm neck: 1.2 mm;
- Height of the secondary aneurysm: 0.7 mm.

As for the above specified values of parameters, the shape coefficient λ and the size coefficient μ were 1.17 and 0.125, respectively. Thereby, the aneurysm was located within the transitional zone and it was necessary to perform the follow-up test within a shorter period than the planned one by neurosurgeon due to the increased rupture risk of the aneurysm. Location of the aneurysm in the initial growth phase is denoted as $\square 1$ in Fig. 8.

The follow-up test showed that width of the secondary aneurysm neck was 2.6 mm, height of the secondary aneurysm was 2.8 mm, radius of the primary aneurysm was 6.3 mm, and width of the primary aneurysm neck was 7.91 mm. As for those parameters, the shape coefficient λ and the size coefficient μ were 2.154 and 0.206, respectively, and the aneurysm was located in the rupture zone. Location of the aneurysm in the second growth phase is denoted as $\square 2$ in Fig. 8. Taking into account the results of simulations, i.e. occurrence of the wall shear stresses exceeding $10 \text{ dyn} \cdot \text{cm}^{-2}$ in the area of the blood impingement at the neck of the primary aneurysm for curvature of the artery higher than 0.1 mm^{-1} , and the area of the blood impingement at the neck twice as large as the area of blood impingement of the aneurysm located on the artery of 0.1 mm^{-1} curvature, this case must be immediately treated surgically due to high rupture risk of the secondary aneurysm, and consequently of the primary aneurysm. The aneurysm ruptured 4 months after the last follow-up test and was successfully embolised.

4.2. Sidewall Aneurysm of Large Neck Width Located on Artery of Medium Curvature

Using images from the spiral CT, the following geometrical parameters of the aneurysm and the artery in the initial growth phase of the secondary aneurysm were determined:

- Curvature of the artery on which the primary aneurysm was located: 0.1 mm^{-1} ;
- Width of the primary aneurysm neck: 9.7 mm;
- Radius of the primary aneurysm: 5.4 mm;
- Width of the secondary aneurysm neck: 1.8 mm;
- Height of the secondary aneurysm: 0.4 mm.

As for the above specified values of parameters, the shape coefficient λ and the size coefficient μ were 0.444 and 0.167, respectively. Thereby, the aneurysm was located within the secure zone. Location of the aneurysm in the initial growth phase is denoted as O 1 in Fig. 8.

The follow-up test showed that width of the secondary aneurysm neck was 3,4 mm, height of the secondary aneurysm was 2.2 mm, radius of the primary aneurysm was 6.2 mm, and width of the primary aneurysm neck was 10.12 mm. As for those parameters, the shape coefficient λ and the size coefficient μ were 1.294 and 0.274, respectively, and the aneurysm was located in the transitional zone. Location of the aneurysm in the second growth phase is denoted as O 2 in Fig. 8.

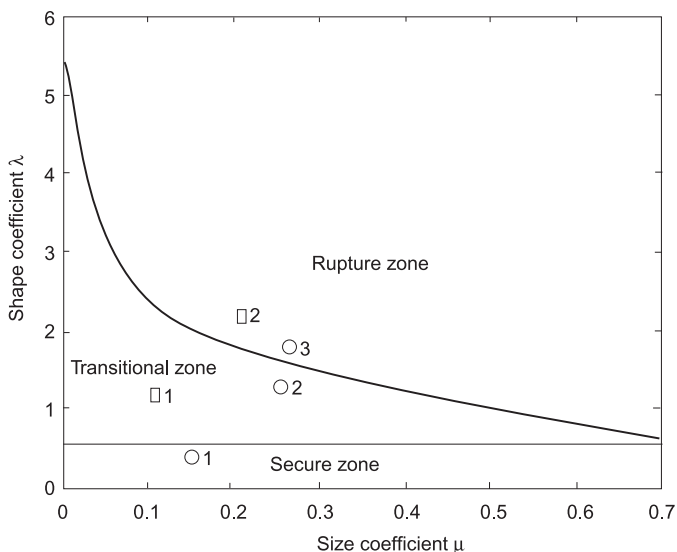


Fig. 8. Identification of the rupture risk of the sidewall aneurysm of small neck width on the artery of high curvature (□ 1 and □ 2) and of the sidewall aneurysm of large neck width on the artery of medium curvature (O 1, O 2 and O 3)

The next follow-up test showed that width of the secondary aneurysm neck was 3.8 mm, height of the secondary aneurysm was 3.6 mm, radius of the primary aneurysm was 6.6 mm, and width of the primary aneurysm neck was 11.2 mm. As for those parameters, the shape coefficient λ and the size coefficient μ were 1.895 and 0.288, respectively, and the aneurysm was located in the rupture zone. Location of the aneurysm in the third growth phase is denoted as O3 in Fig. 8. Taking into account the results of simulations, i.e. occurrence of the wall shear stresses exceeding $10 \text{ dyn} \cdot \text{cm}^{-2}$ in the area of the blood impingement at the neck of the primary aneurysm of width larger than 8 mm, and relatively high curvature of the artery equal to 0.1 mm^{-1} , this case must be immediately treated surgically due to high rupture risk of the secondary aneurysm, and consequently of the primary aneurysm. The aneurysm ruptured 3 months after the last follow-up test and was successfully embolised.

5. Conclusions

The results of the tests related to static and dynamic properties of the intracranial aneurysms and the model of growth of the primary and the secondary aneurysm can be used in further researches leading to elaboration of the decision-making system helpful for neurosurgeons. Analysis of parameters such as artery curvature, wall shear stress, relative tensile stress and size of the area of elevated wall shear stress has made possible to assess the rupture risk of five clinical cases of the primary and the secondary aneurysm. The results are absolutely essential for neurosurgeons, as one of the tested aneurysms was in the state of relative stability and did not rupture, whereas three aneurysms were located in the rupture zone and actually ruptured a few months after the follow-up test. The exception was the case of the aneurysm of the medium neck width located on the artery of medium curvature, as there was a discrepancy between the criterion qualifying the aneurysm to the transitional zone and the clinical evidence (the aneurysm ruptured shortly after the follow-up test). Therefore, it has been proved that analysis of the rupture risk solely on the criterion of size of the primary aneurysm and occurrence of the subarachnoid hemorrhage is not reliable due to omission of aspects of hemodynamics of blood in the aneurysm and the artery, as well as stresses related to the secondary aneurysms. These extra factors guarantee a more precise assessment of the rupture risk of aneurysms and provide a perfect basis for elaboration of the decision-making system.

Acknowledgments

The author expresses gratitude to doctors from the Regional Public Hospital in Szczecin for their valuable remarks and professional advices related to the complex matter of the intracranial aneurysms.

References

1. Van Gijn J., Rinkel G.: Subarachnoid hemorrhage: diagnosis, causes and management. *Brain* 2001, 124, 249–278.
2. Forget T.R. Jr, Benitez R., Veznedaroglu E., et al.: A review of size and location of ruptured intracranial aneurysms. *Neurosurgery* 2001, 49(6), 1322–1326.
3. Rogers L.: Intracranial aneurysm size and potential for rupture. *J. Neurosurg* 1987, 67, 475–476.
4. Schievink W.I., Piepgras D.G., Wirth F.P.: Rupture of previously documented small asymptomatic saccular intracranial aneurysms. *J. Neurosurg.* 1992, 76, 1019–1024.
5. Burlison A.C., Strother C.M., Turitto V.T.: Computer modeling of intracranial saccular and lateral aneurysms for the study of their hemodynamics. *Neurosurgery* 1995, 37, 774–782.
6. Batjer H.H., Samson D.S.: Basilar bifurcation aneurysm. *The Practice of Neurosurgery*, Baltimore, Williams and Wilkins 1996, 2261–2270.
7. Ho H., Crute D., Batjer H.H.: Surgical techniques for intracranial aneurysms. *Principles of Neurosurgery*, Second Edition. Philadelphia, Lippincott-Raven Publishers 1999, 311–337.
8. Sundt T.M. Jr, Kobayashi S., Fode N.C., Whisnant J.P.: Results and complications of surgical management of 809 intracranial aneurysms in 722 cases. Related and unrelated to grade of patient, type of aneurysm, and timing of surgery. *J. Neurosurg.* 1982, 56, 753–765.
9. Wirth F.P.: Surgical treatment of incidental intracranial aneurysm. *Clin. Neurosurg.* 1986, 33, 125–135.
10. Ford M.D., Stuhne G.R., Nikolov H.N., Habets D.F., Lownie S.P., Holdsworth D.W., Steinman D.A.: Virtual angiography for visualization and validation of computational models of aneurysm hemodynamics. *IEEE Trans. Med. Imaging* 2005, 24(12), 1586–1592.
11. Foutarakis G.N., Yonas H., Sclabassi R.J.: Saccular aneurysm formation in curved and bifurcating arteries. *AJNR Am. J. Neuroradiol.* 1999, 20, 1309–1317.
12. Kumar B.V., Naidu K.B.: Hemodynamics in aneurysm. *Computers and Biomedical Research* 1996, 29, 119–139.
13. Metcalfe R.W.: The promise of computational fluid dynamics as a tool for delineating therapeutic options in the treatment of aneurysms. *AJNR Am. J. Neuroradiol.* 2003, 24, 553–554.
14. Shojima M., Oshima M., Takagi K., Torii R., Hayakawa M., Katada K., et al.: Magnitude and role of wall shear stress on cerebral aneurysm. *Computational Fluid Dynamic study of 20 middle cerebral artery aneurysms.* *Stroke* 2004, 35, 2500–2505.
15. Stuhne G.R., Steinman D.A.: Finite element modeling of the hemodynamics of stented aneurysms. *J. Biomech. Eng.* 2004, 126(3), 382–387.
16. Kerber C.W., Heilman C.B.: Flow in experimental berry aneurysms: method and model. *AJNR Am. J. Neuroradiol.* 1983, 4(3), 374–377.
17. Liepsch D.W., Steiger H.J., Poll A., Reulen H.J.: Hemodynamic stress in lateral saccular aneurysms. *Biorheology* 1987, 24, 689–710.
18. Nagayasu S., Kikuchi H., Nagasawa S., Ohtsuki H.: Basilar artery occlusion therapy for giant aneurysm: hemodynamic analysis by hydraulic vascular model. *No Shinkei Geka* 1992, 20(11), 1161–1167.
19. Yamaguchi K., Nagasawa S., Kawabata S., Kawanishi M., et al.: Paraclinoid aneurysms of the internal carotid artery: hydraulic simulation study on their locations and shape of the carotid siphon. *Neurol. Res.* 1999, 21(8), 733–736.
20. Steiger H.J., Liepsch D.W., Poll A., Reulen H.J.: Hemodynamic stress in terminal saccular aneurysms: A laser-Doppler study. *Heart Vessels* 1988, 4, 162–169.
21. Tateshima S., Murayama Y., Villablanca J.P., Morino T., et al.: In vitro measurement of fluid-induced wall shear stress in unruptured cerebral aneurysms harboring blebs. *Stroke* 2003, 34(1), 187–192.
22. Di Martino E.S., Guadagni G., Fumero A., Ballerini G., Spirito R., Biglioli P., et al.: Fluid-structure interaction within realistic three-dimensional models of the aneurysmatic aorta as a guidance to assess the risk of rupture of the aneurysm. *Med. Eng. Phys.* 2001, 23, 647–655.

23. Tateshima S., Murayama Y., Villablanca J.P., Morino T., et al.: Intraaneurysmal flow dynamics study featuring an acrylic aneurysm model manufactured using a computerized tomography angiogram as a mold. *J. Neurosurg.* 2001, 95, 1020–1027.
24. Villablanca J.P., Jahan R., Hooshi P., Lim S., et al.: Detection and characterization of very small cerebral aneurysms by using 2D and 3D helical CT angiography. *AJNR Am. J. Neuroradiol.* 2002, 23, 1187–1198.
25. Jou L.D., Quick C.M., Young W.L., et al.: Computational approach to quantifying hemodynamic forces in giant cerebral aneurysms. *AJNR Am. J. Neuroradiol.* 2003, 24(9), 1804–1810.
26. Satoh T., Onoda K., Tsuchimoto S.: Visualization of intraaneurysmal flow patterns with transluminal flow images of 3D MR angiograms in conjunction with aneurysmal configurations. *AJNR Am. J. Neuroradiol.* 2003, 24, 1436–1445.
27. Aoki N., Kitahara T., Fukui T., et al.: Management of unruptured intracranial aneurysm in Japan: a Markovian decision analysis with utility measurements based on the Glasgow Outcome Scale. *Med. Decis Making* 1998, 18, 357–364.
28. Johnston S.C., Gress D.R., Kahn J.G.: Which unruptured cerebral aneurysms should be treated? A cost-utility analysis. *Neurology* 1999, 52, 1806–1815.
29. Leblanc R., Worsley K.J.: Surgery of unruptured, asymptomatic aneurysms: a decision analysis. *Can. J. Neurol. Sci.* 1995, 22, 30–35.
30. Mitchell P., Jakubowski J.: Risk analysis of treatment of unruptured aneurysm. *J. Neurol. Neurosurg. Psychiatry* 2000, 68, 577–580.
31. Yoshimoto Y., Wakai S.: Cost-effectiveness analysis of screening for asymptomatic, unruptured intracranial aneurysms. A mathematical model. *Stroke* 1999, 30, 1621–1627.
32. Abruzzo T., Shengelaia G.G., Dawson III R.C., Owens D.S., Cawley C.M., Gravanis M.B.: Histologic and morphologic comparison of experimental aneurysms with human intracranial aneurysms. *AJNR* 1998, 19, 1309–1314.
33. Frerichs K.U., Stieg P.E., Friedlander R.M.: Prediction of aneurysm rupture site by an angiographically identified bleb at the aneurysm neck. *J. Neurosurg.* 2000, 93, 517.
34. Crompton M.R.: Mechanism of growth and rupture in cerebral berry aneurysms. *British Journal of Neurosurgery* 1966; 1(5496), 1138–1142.
35. Sampei T., Mizuno M., Nakajima S., Suzuki A., Hadeishi H., Ishikawa T., Yasui N.: Clinical study of growing up aneurysms: report of 25 cases. *No Shinkei Geka* 1991, 19, 825–830.
36. Steiger H.J.: Pathophysiology of development and rupture of cerebral aneurysms. *Acta Neurochir. Suppl. (Wien)*, 1990, 48, 1–57.
37. Meng H., Feng Y., Woodward S.H., Bendok B.R., Hanel R.A., Guterman L.R., Hopkins L.N.: Mathematical model of the rupture mechanism of intracranial saccular aneurysms through daughter aneurysm formation and growth. *Neurological Research* 2005, 27, 459–465.
38. Szafranski K.: Analysis of rupture of intracranial saccular aneurysms, 6th IFAC Symposium on Modelling and Control in Biomedical Systems MCBMS'06, Reims 2006, 495–500, ISBN-10: 0080445306.
39. Aenis M., Stancampiano A.P., Wakhloo A.K., Lieber B.B.: Modeling of flow in a straight-stented and non-stented side wall aneurysm model. *J. Biomech. Eng.* 1997, 119, 206–212.
40. Foutarakis G.N., Yonas H., Sclabassi R.J.: Saccular aneurysm formation in curved and bifurcating arteries. *AJNR Am. J. Neuroradiol.* 1999, 20, 1309–1317.
41. Kumar B.V., Naidu K.B.: Hemodynamics in aneurysm. *Computers and Biomedical Research* 1996, 29, 119–139.
42. Szafranski K.: Analysis of hemodynamics of intracranial saccular aneurysms. 29th Annual International Conference of the IEEE Engineering in Medicine and Biology Society EMBC 2007, Lyon 2007, ID 2859, ISBN: 1-4244-0788-5.
43. Hoi Y., Meng H., Woodward S.H., Bendok B.R., Hanel R.A., Guterman L.R., Hopkins L.N.: Effects of arterial geometry on aneurysm growth: three-dimensional computational fluid dynamics study. *J. Neurosurg.* 2004, 101, 676–681.

44. Gijsen F.J.H., Vosse F.N. van de, Janssen J.D.: The influence of the non-Newtonian properties of blood on the flow in large arteries: steady flow in a carotid bifurcation model. *J. Biomech.* 1999, 32, 601–608.
45. Hassan T., Timofeev E.V., Saito T., Shimizu H., Ezura M., Tominaga T., et al.: Computational replicas: anatomical reconstructions of cerebral vessels as volume numerical grids at three-dimensional angiography. *AJNR Am. J. Neuroradiol.* 2004, 25, 1356–1365.
46. Steiger H.J., Poll A., Liepsch D., Reulen H.J.: Basic flow structure in saccular aneurysms: A flow visualization study. *Heart Vessels* 1987, 3, 55–65.